Automatic Control of Arc Welding (Report II)†
—Optical Sensing of Joint Configuration—

Yoshiaki ARATA* and Katsunori INOUE**

Abstract

A new method has been developed, in which an optical sensor was utilized for sensing and monitoring the joint configuration during arc welding. This method is characterized by using the light which is emitted from the welding arc. Using this sensing method, the position of the electrode in space relative to the joint axis and the joint preparation (the groove width and depth, etc.) can be sensed in the arcing zone during the welding process.

Sensing resolution can be very fine provided that an optical system is properly chosen. Sensing ability depends on the welding condition, such as arc voltage and arc current.

This dependency was investigated experimentally and the sensing ability index was obtained from the experimental results following the special formula described later.

This index can give the universal data for the design of the joint configuration sensor of this type.

1. Introduction

Introducing and developing a new automatic joint sensing and tracking system in the arc welding process have been greatly needed in recent years, and several methods have been reported.[1), 2), 3)]

The common disadvantage to the sensing systems that have been developed was that they were never able to discriminate the joint at the arcing zone during the welding process, because the sensors are affected by heat, light, sound, electric and magnetic noise, spattering and so on, generated during welding.

Therefore, in these systems, the sensors are usually located 50～100 [mm] away from the welding heads. Thus, sensing and tracking systems have a tendency to be complicated and expensive, moreover, tracking accuracy is diminished.

In order to solve such difficulties, a new method which makes it possible to sense the joint configuration at the arcing zone has been developed.

In this method, the image of the joint in the vicinity of the welding arc appears on the focusing of the optical pattern receiver installed on the welding head, and various characteristic parameters of such image are converted into electrical signals by photoelectric elements located at the screen and the logic systems connecting them. In this position, the sensor is not affected by the disturbances such as heat, light, noise, and moreover, spattering disturbance can be protected with a conventional gas curtain, because the sensing system is located considerable distance away from the arc.

From the various characteristic parameters of the image, the horizontal deviation of the wire from the weld line, E, the clearance between the work piece and the torch nozzle, Z, the joint preparation parameters B (groove width) and the others can be sensed.

Sensing resolution of such values can be very fine provided that an optical system is properly chosen and the condition of the welding arc as the light source for the image is good. In case the arc condition is bad (from the viewpoint of the joint configuration sensing), the image flickers and the sensed electrical signal fluctuates. The sensing ability of the joint configuration depends on the welding condition, especially on the arc voltage and the current, because the welding arc is the only light source for the image.

For this reason, it is necessary to define the sensing ability index for the image which depends on the arc condition. The index is computed by following a particular formula.

2. Principles of Sensing

Figure 1 shows the fundamental diagram of the sensing apparatus. The holder installed on the welding head can rotate around the center axis of the welding head, and its horizontal plane angle θ can be regulated by the servo-mechanism. The holder supports the pattern receiver. The optical axis of the pattern receiver looks towards the tip of the electrode (the welding wire), so that the light of the welding arc

† Received on Nov. 25, 1972

* Professor

** Research Associate, Department of Welding Engineering, Faculty of Engineering, Osaka University

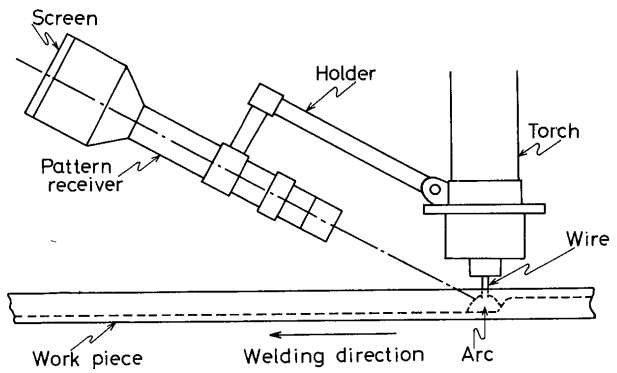

Fig. 1. Schematic of fundamental sensing apparatus.

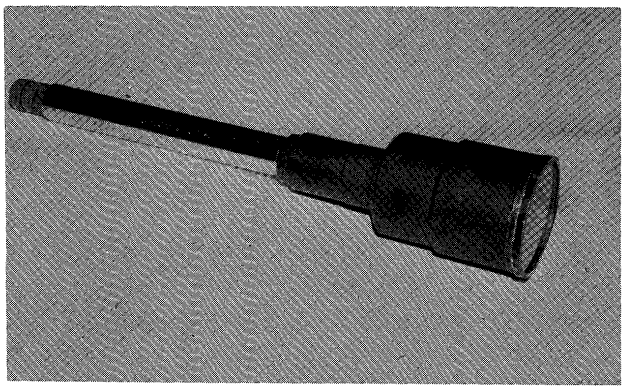

Photo. 1. Appearance of pattern receiver.

throws an image of any objects which exist in the vicinity of the tip of the electrode, on the focusing screen of the pattern receiver through its lens. The vertical angle of the pattern receiver optical axis can be regulated arbitrarily from 0[°] to about 65[°].

Photograph 1 indicates the appearance of the pattern receiver. The magnifying power of the receiver is 4.5 in this study.

Photographs 2, 3, 4 and **5** show some examples of the images on the focusing screen of the pattern receiver. While photographing the images, the welding torch is fixed and the work is moved if necessary. The images by TIG arc are shown in **Photos. 2** and **3,** where TIG arc was generated on the groove model of water cooled copper. **Photograph 2** shows the images for the square groove, (a), (b) and (c) correspond to the case, where the vertical plane angle φ of the pattern receiver optical axis is equal to 0°, 45° and 60° respectively.

The image of the groove is definite and shows both sides of the groove edge, therefore, the groove width can be easily detected and converted into electrical signal by any means. The contour map for photographic density of **Photo. 1 (c)** by micro-photometer scanning are shown in **Fig. 3.** The images for the bevel groove whose groove angle is 90° are shown

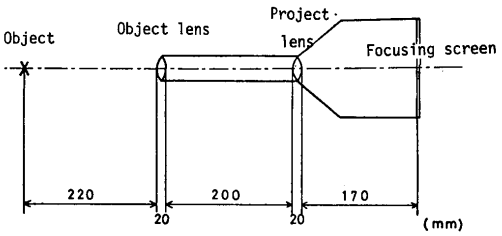

Fig. 2. Schematic of optical system – pattern receiver.

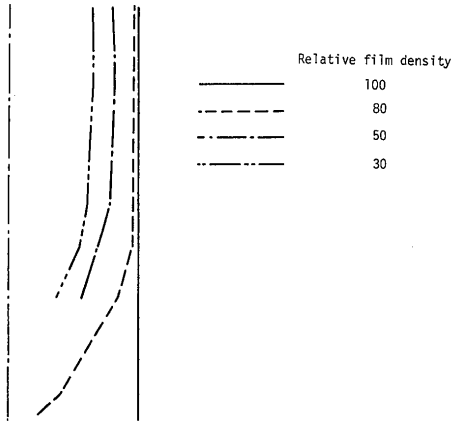

Fig. 3. Contour map for photographic density with microphotometer scanning of Photo. 1 (c).

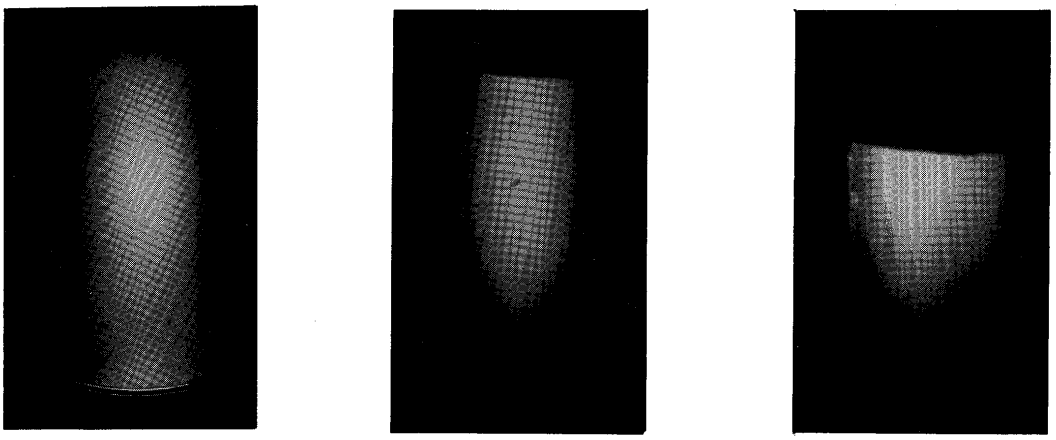

(a) (b) (c)

Photo. 2. Images for square groove by TIG arc from various aiming angles φ. (a) φ=0°, (b) φ=30°, (c) φ=45°.

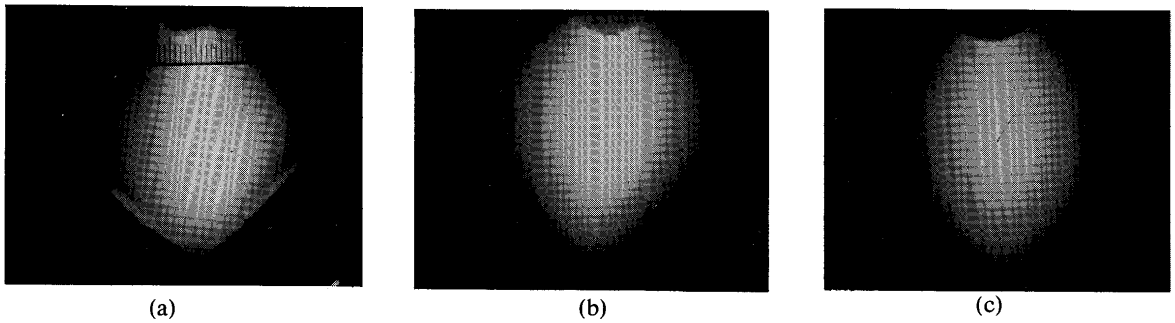

(a) (b) (c)

Photo. 3. Images for bevel groove by TIG arc from various aiming angles φ. (a) $\varphi=0°$, (b) $\varphi=30°$, (c) $\varphi=45°$.

in **Photo. 3,** where (a) $\varphi=0°$, (b) $\varphi=30°$ and (c) $\varphi=45°$ respectively.

The micro-photo-meter scanning contour maps corresponding to **Photo. 3 (a), (b)** and **(c)** are also shown in **Fig. 4 (a), (b)** and **(c).**

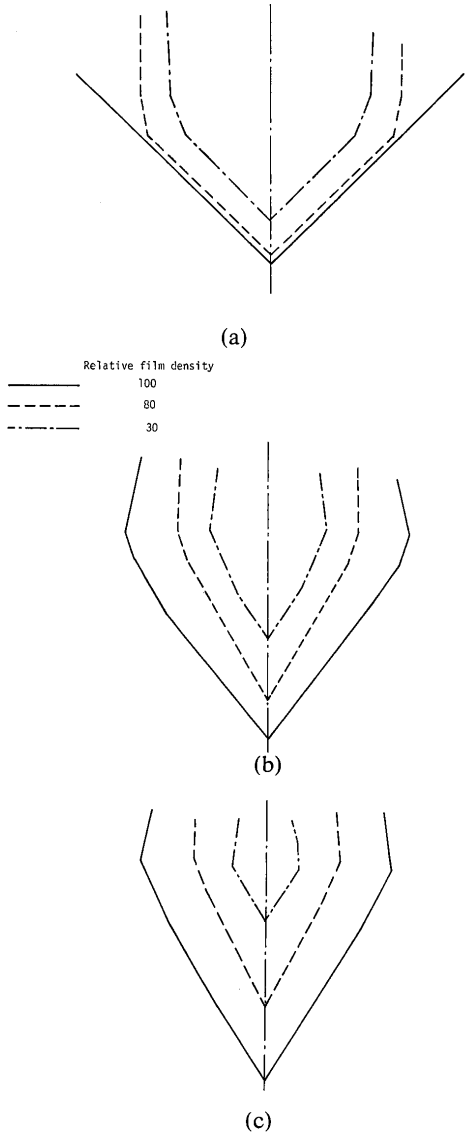

Fig. 4. Contour maps for photographic density.
(a) scanning of Photo. 3 (a)
(b) scanning of Photo. 3 (b)
(c) scanning of Photo. 3 (c)

As is seen in **Photo. 3 (a), (b)** and **(c),** when the vertical angle increases, the image becomes more indefinite in the case of the bevel groove.

Examples of the image by a consumable electrode arc are shown in **Photos. 4** and **5.**

The images of the square groove are shown in **Photo. 4 (a), (b)** and **(c),** where (a) and (b) are the images by CO_2 arc, (c) is by MIG arc. The electrode (the wire) is centered in **Phot. 4 (a),** and off-center in **Photo. 4 (b).** The images in **Photo. 4** are more definite than in **Photo. 2.** There is no remarkable difference between the image by CO_2 arc and by MIG arc.

The images of the bevel groove are shown in **Photo. 5, (a), (b), (c)** and **(d),** where the shielding gas mixture ratio is diffrent as follows: (a) CO_2=100 %, (b) Ar: CO_2=50 % : 50 %, (c) Ar : CO_2=75 % : 25 %, (d) Ar=100 %, the other welding conditions (arc voltage 30 [V], arc current 350 [A] and welding speed 300 [mm/min]) and the observation direction angle ($\theta=0°$ and $\varphi=25°$) is the same, except that the arc voltage in (d) is 24 [V].

It is seen from **Photo. 5** that the image of the bottom of the bevel groove becomes angular as Ar gas mixture ratio increases. The properties of the image pattarn as mentioned above can be qualitatively explained by the simple drawing shown in **Figs. 5, 6** and **7.**

At first, we assume the external appearance of the arc as a right circular cone as shown in (a) of **Figs. 5, 6** and **7.** The circular cone is sliced by the plane of the groove face. The intersection line of the slicing plane and the cone surface gives the joint configuration pattern. Its projection on the plane whose nomal line is equivalent to the pattern receiver optical axis corresponds to the image on the focusing screen.

Figure 5 is the example for the bevel groove. The right circular cone is sliced by the two planes T and T_1 which are at an angle 45 [°] to the horizontal plane and meet at an angle of 90 [°] each other (this is equivalent to groove angle 90 [°] as shown in (a).

The side view and the plane view of the cone with

(a) (b) (c)

Photo. 4. Images for square groove by CO_2 arc and MIG arc.
(a) Image by CO_2 arc-wire is centred at groove zone.
(b) Image by CO_2 arc-wire is deviated at groove zone.
(c) Image by MIG arc.

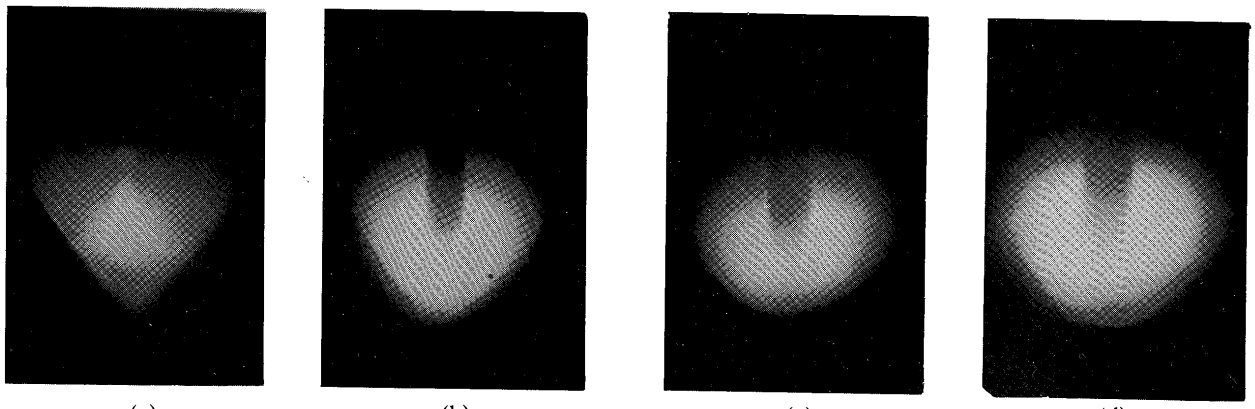

(a) (b) (c) (d)

Photo. 5. Change of image for bevel groove with gas mixture ratio. (a) Ar: 100 %, (b) Ar: 75 % CO_2: 25 %, (c) Ar: 50 % CO_2: 50 %, (d) CO_2: 100 %.

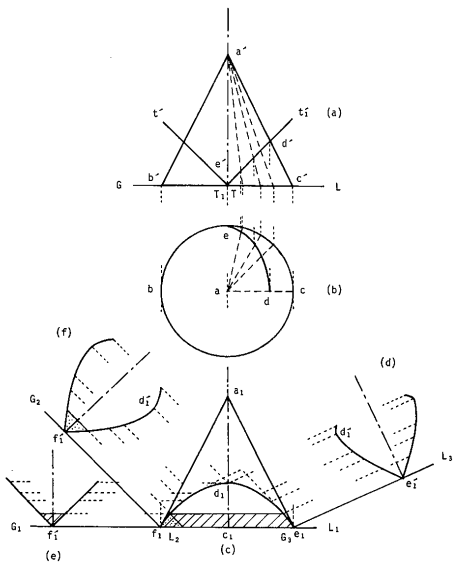

Fig. 5. Drawing to explain image of groove configuration.

the intersection line are shown in (b) and (c) respectively. The projections on the planes whose normal lines are at an angle of 25°, 0° and 45° to the horizontal plane (as the vertical angle) are shown in (d), (e) and (f). From **Fig. 5** it can easily be understood why the image in (e) and also in **Photo. (2) (a)** where $\varphi=0$ gives the correct value of groove angle, but the images in (d), (f) and also in **Photos. 2 (b), (c)** and **5** where $\varphi \neq 0$ give considerably smaller value.

The reason why the image becomes more undefinite as the projection angle (the vartical angle φ) increases, as was seen in **Photo. 3,** can be explained by the fact that the light emitted from the arc plasma, which exists at the shadowed portion in **Fig. 5 (c);** contributes to the formation of the image shadowed in **Fig. 5 (e),** on the other hand, the small plasma arc, which exists at the dotted

protion in **Fig. 5** (c), contributes to the formation of the image dotted in **Fig. 5** (e). The image pattern difference among **Photo. 5 (a), (b), (c)** and **(d)** can be explained as follows. The penetration effect of CO_2 arc is greater than that of MIG arc so that the drawing should be made as shown in **Fig. 6** instead of **Fig. 5,** in which the circular cone is sliced by the planes P_3 and P_4 instead of P_1 and P_2 (see **Fig. 6** (a)) in case the mixture ratio of CO_2 gas increases in quantity. The projected image looks roundish at its pointed end as shown in **Fig. 6** (d).

The drawing corresponding to the square groove is shown in **Fig. 7.** It is seen from **Fig. 7 (d)** and **(e)** that the projected image gives the correct groove width regardless of the projection angle and the penetration effect of the welding arc.

It is clear from the above consideration that the principle developed here is most suitable for sensing the square groove including the narrow gap. For this reason, we limit our chief discussion to sensing the square groove in the remainder of this report.

The typical joint design of the square groove and values to be sensed are shown in **Fig. 8,** where B is the groove width, E ($=B_1 \sim B_2$) is the horizontal deviation of the wire from the weld line, Z is the clearance between the work piece and the torch nozzle. **Figure 9** shows a typical pattern of the image.

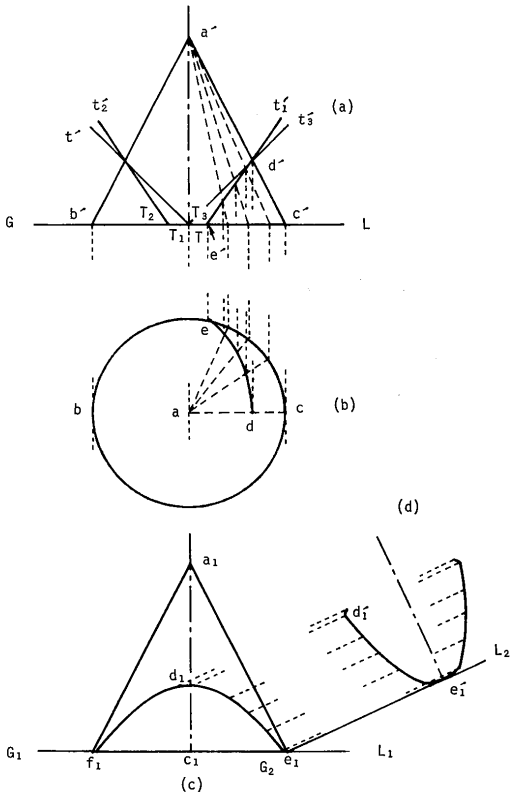

Fig. 6. Drawing to explain image of groove configuration.

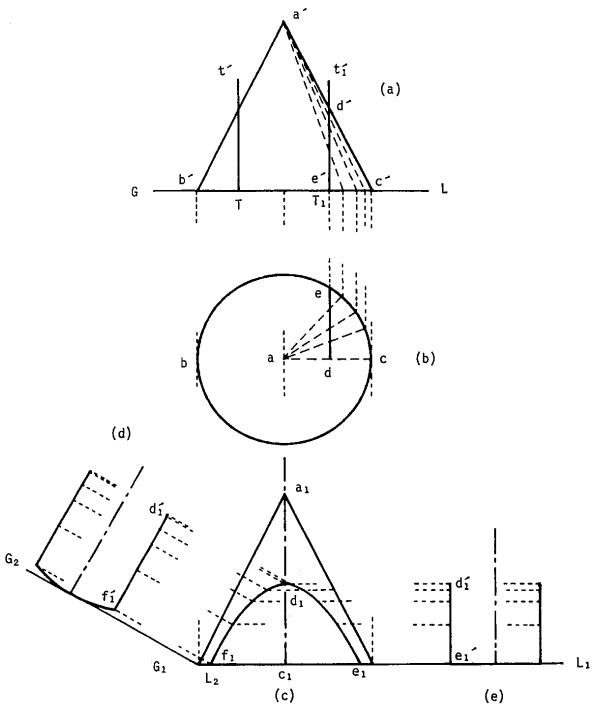

Fig. 7. Drawing to explain image of groove configuration.

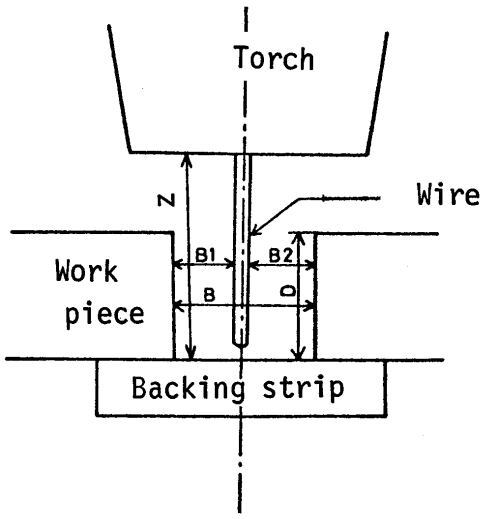

Fig. 8. Typical joint design and values for sensing.

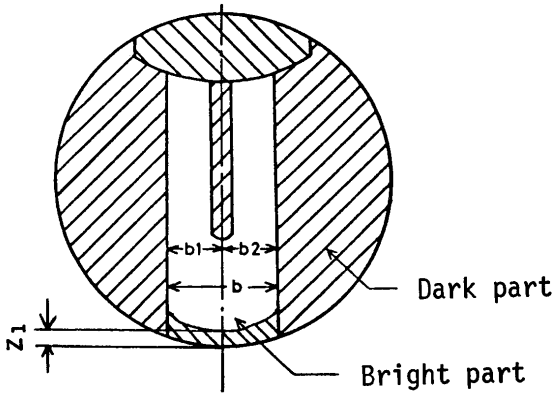

Fig. 9. Typical pattern of image.

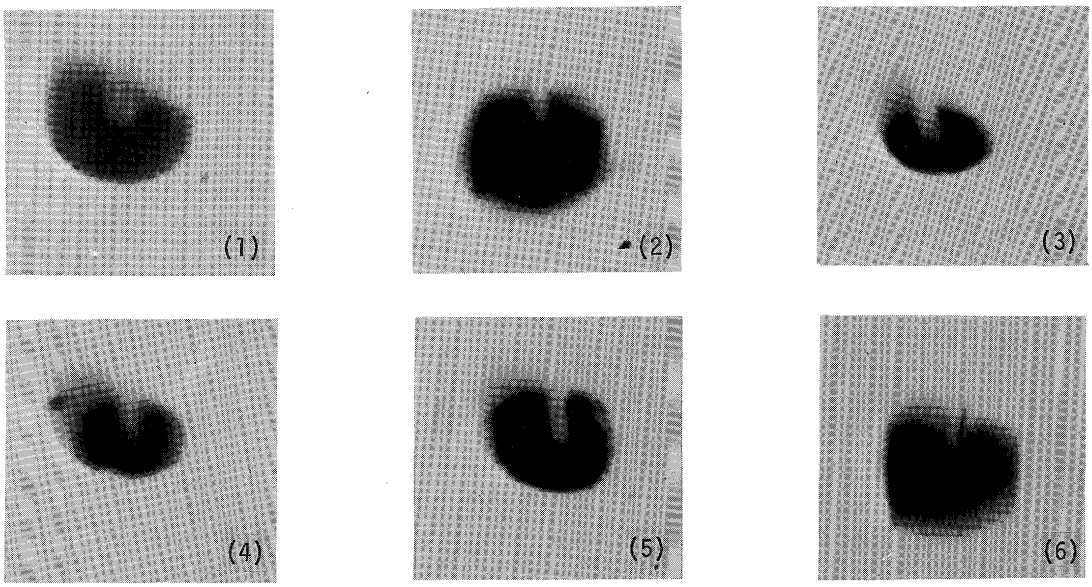

Photo. 6. Change of image at each moment.

The symbols b, b_1 and b_2 which are given to the image, correspond to B, B_1 and B_2 in **Fig. 8,** Z in **Fig. 8** must be estimated by sensing Z_1 in **Fig. 9,** neglecting the difference of the penetration effect by arc condition.

3. Characteristics of Joint Configuration Image

The joint configuration image on the screen during arc welding process was photographed with a cine-camera. One example is shown in **Photo. 6,** in which CO_2 arc welding was made on a square grooved work piece whose width was 9 [mm], at arc current 350 [A], arc voltage 26 [V] and travel speed 400 [mm/min].

The photograph was taken at the rate of one frame per second with shutter speed of 1/36 [sec]. Each frame shows a slightly different pattern owing to fluctuation of the arc.

The image of CO_2 arc varies every moment in such a manner that sensing the joint configuration by CO_2 arc is more difficult than by MIG arc.

For this reason, characteristics of the image by CO_2 arc are investigated first.

The variations of the image pattern by CO_2 arc are also shown in **Photo. 7.** It is seen that the image pattern depends on the welding condition.

The experiment for which a schematic diagram is shown in **Fig. 10** was made to test quantitatively the sensitivity of the image.

In this experiment, the image at each moment was photographed on 8 [mm] cinefilm (18 frames per sec.) previously and reproduced on the screen by a projector. The photoelectric elements (silicon-photo-diode) composed of ten segments are installed on the screen as seen in **Fig. 10.** Each segment and the

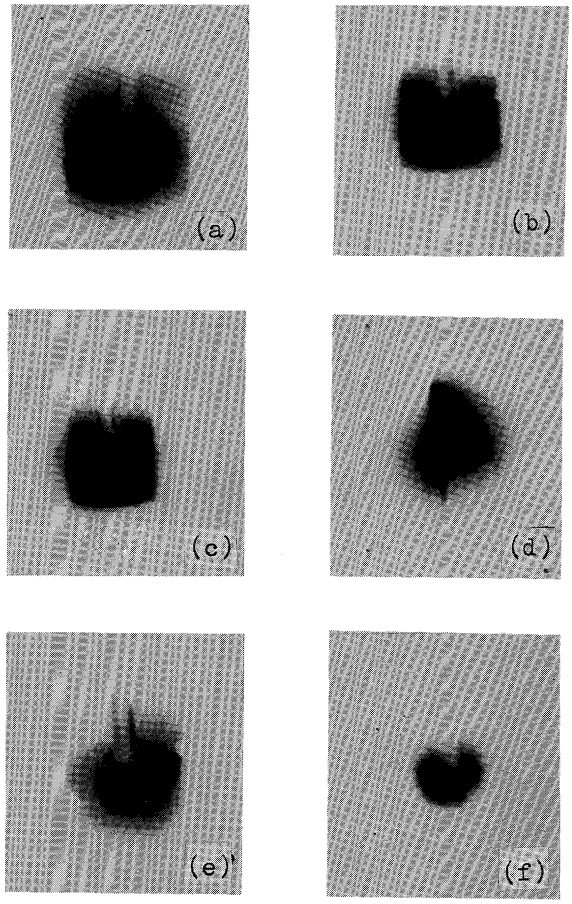

Photo. 7. Examples (a), (b) and (c) of desirable images, (d) for wire deviating, (e) by too small arc current and (f) by too low arc voltage.

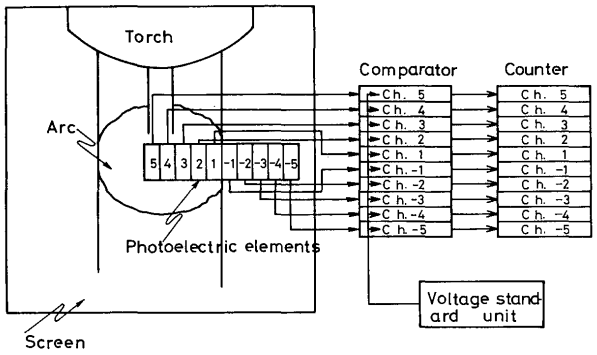

Fig. 10. Schematic diagram of experiment on joint sensibility.

following system are represented in channel number from Ch.−5 to Ch.5.

When the image is reproduced, each photoelectric element generates the pulse whose frequency is equivalent to the reproduced numbers of frames per second, and whose pulse height corresponds to the brightness of the image where that photoelectric element exists.

The output pulse is discriminated by the voltage comparator which is connected to each photoelectric element. The discriminating level of the voltage comparator can be set by the voltage standard unit at an arbitrary value.

The counter acts each time that the output signal of the voltage comparator turns from high level to low level and counts its turning frequency so that the counting rate of each channel in a reproducing period indicates the numbers of frames in which the brightness of the image is over a certain preset discriminating level in the part of that channel.

The cine-photographs were taken for various arc voltage, arc current of CO_2 welding on various groove width work pieces and count rate data were obtained from these photographs.

Some examples of the counting rate are shown in **Fig. 11.** In this figure, channel no. −1 ～ −5 and channel no. 1～5 which are plotted on the abscissa correspond to the outside and inside of the groove image respectively; the counting rate which is plotted on the ordinate is expressed as a percentage of counted numbers of frames to all projected frames, position number expresses the relative vertical position of the photoelectric elements on the screen, and discriminating level is denoted in arbitrary unit which is nearly proportional to intensity of illumination.

It is seen from **Fig. 11** that the proper vertical position for the photoelectric elements and the proper discriminating level for the voltage comparators are necessary to obtain the correct groove configuration. (For example, the position no. 3 and the discriminating level 300 are proper in **Fig. 11**). The obtained counting rate data were substituted into the formula (eq. 1) and the sensibility indexes were calculated out.

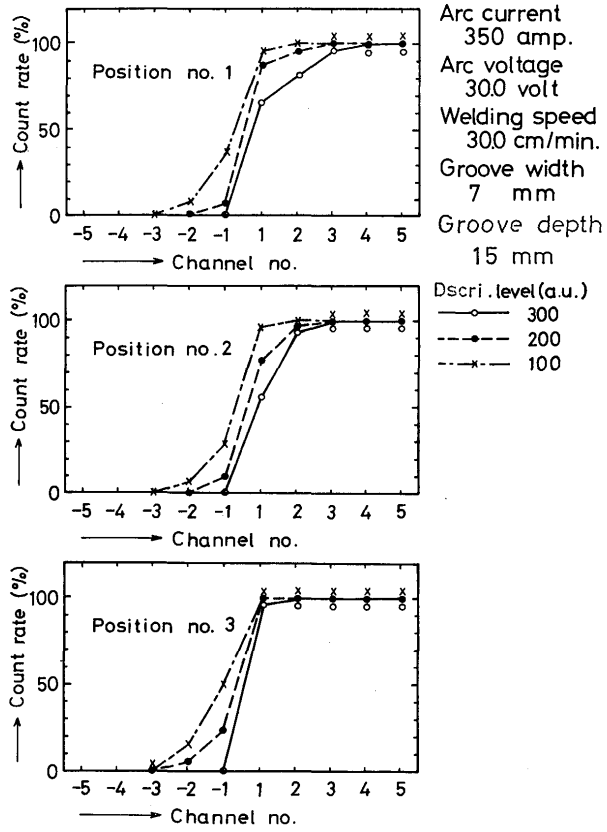

Fig. 11. Some examples of counting rate data.

Equation 1 is the formula introduced to treat the image sensibility quantitatively, and is shown as follows:

$$\left.\begin{aligned} I_{total} &= I_{in} + I_{out} \\ I_{in} &= 0.5\,(100.0 - C\,(1)\,) + \sum_{k=2}^{5} k \cdot (100.0 - C\,(k)\,) \\ I_{out} &= 0.5\,C\,(-1) + \sum_{k=2}^{5} k \cdot C\,(-k) \end{aligned}\right\} \text{---- (1)}$$

where I_{in} and I_{out} are the index of inside and outside of the groove images respectively, I_{total} is the total index, C (k) is the counting rate in channel no. k. In the equation of I_{in}, the term of 100.0 minus C (k) expresses miscount to the groove image and is multiplied by the weight that is proportional to the channel no. k, excepting the first trem which is multiplied by 0.5, because the miscount effect becomes more serious as the channel no. k increases. In the equation of I_{out}, C (k) expresses excess-count to the pusedo-image and is multiplied by the weight proportional to the absolute value of the channel number, excepting the first term, in the similar way as in the

equation of I_{in}. If the value of I_{total}, the summnation of I_{in} and I_{out}, is small, the image sensibility is good; inversely, if the value is large, the image sensibility is not good.

Some examples of indexes calculated from the count rate data are shown in **Figs. 12, 13,** and **14.**

In these figures, position number plotted on the abscissa expresses the vertical relative position of the photoelectric elements; the distance between no. k and no. k+1 is equivalent to 2.5 [mm] on the screen and the curves, to which "inside" "outside" are appended, express the index values calculated from I_{in} and I_{out} in eq. 1 respectively. The index depends upon arc power, as well as position number and descriminating level, which can easily be seen from **Fig. 11.**

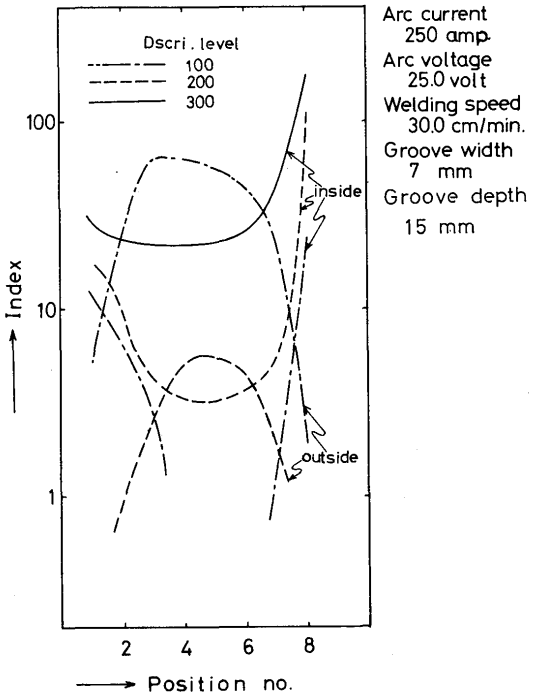

Fig. 12. Example of indexes I_{in} and I_{out}.

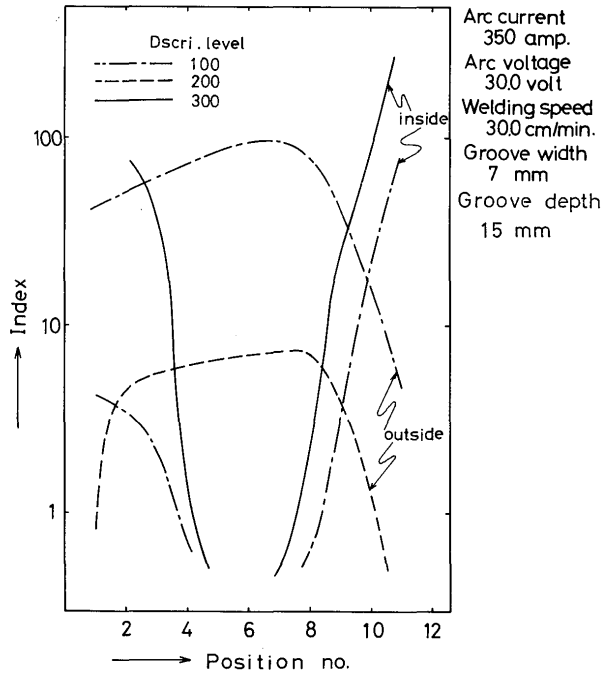

Fig. 13. Example of indexes I_{in} and I_{out}.

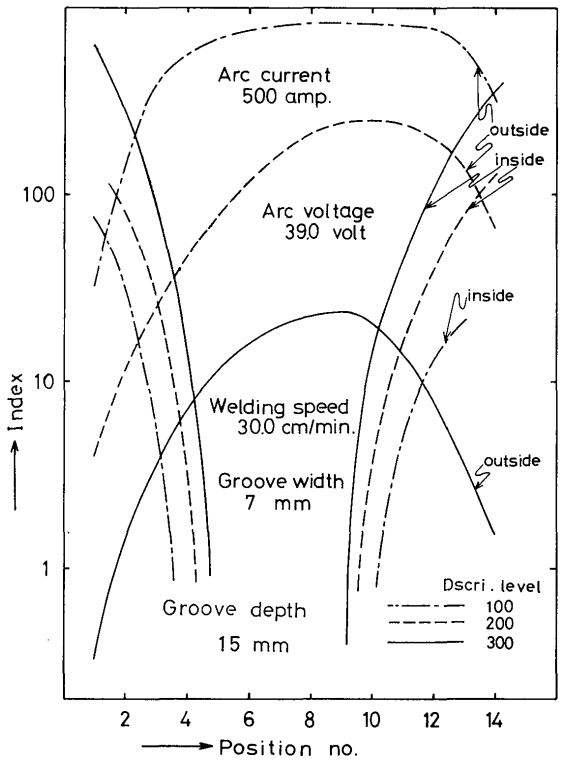

Fig. 14. Example of indexes I_{in} and I_{out}.

Dependency of the index on arc power is shown in **Fig. 15,** in which the curves express I_{total}.

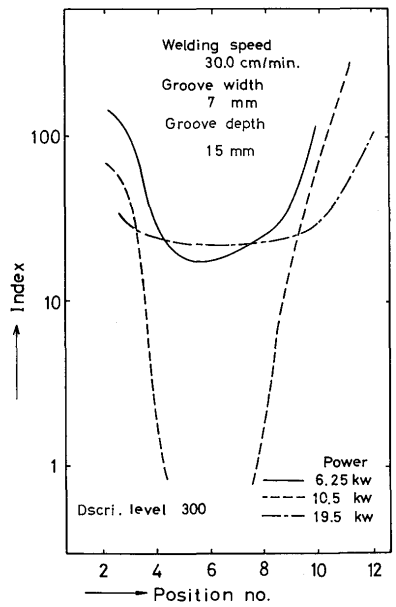

Fig. 15. Dependence of index on arc power.

Three index curves have their minimum values at certain positions. The value of the index must be less than 20 or 30 to make an accurate sensing of joint configuration; therefore the sensing should be made at the minimum index position.

It is expected from **Fig. 15** that the minimum value of the index curve varies depending on arc power under a certain welding condition.

For these reasons, the minimum index value concerned with the position may be defined as the index value under that welding condition.

Figure 16 shows the plot of that kind of index which depends on arc power, when welds were made on three kinds of groove width work piece.

The index curves in **Fig. 16** have a tendency to rise if arc power is small or large for the given groove width; the former case is due to lack of light, and the latter to the excessmelting of the work piece.

Accurate sensing can be assured if arc power is correctly determined for narrow grooves, but considerable sensing error may arise for the wide groove (width 9 [mm]). The index changes with arc voltage for certain arc current and increases for low and high arc voltage as shown in **Figs. 17** and **18.** In the case of low arc voltage, the arc length becomes too short to illuminate the whole groove zone and the arc flickers as the wire short-circuits with the work piece.

In the case of high arc voltage, the arc length becomes too long, the arc becomes unstable and flickers. If arc current is comparatively high, the index curve does not rise so high for high arc voltage as is shown in **Fig. 18.**

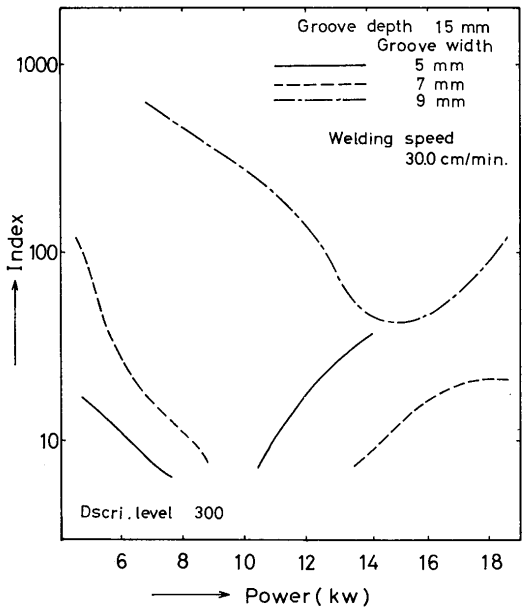

Fig. 16. Dependence of index on arc power and groove width.

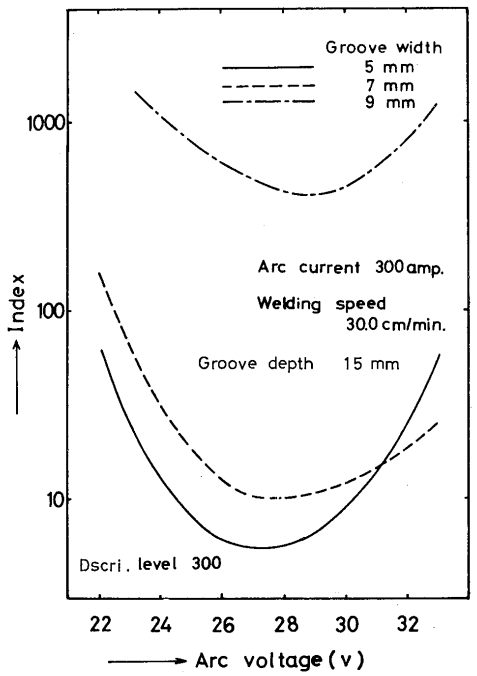

Fig. 17. Dependence of index on arc voltage and groove width.

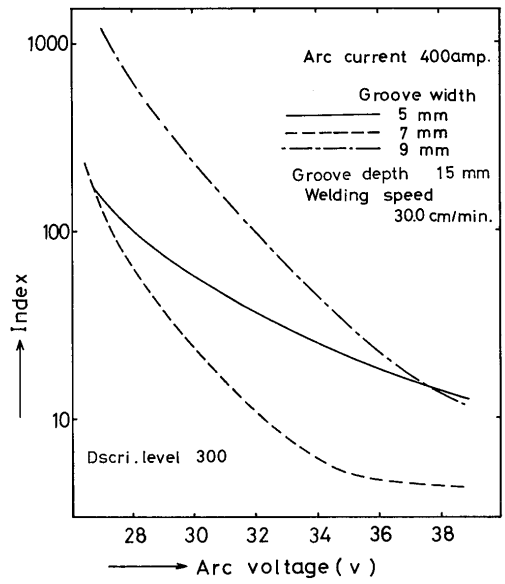

Fig. 18. Dependence of index on arc voltage and groove width.

In **Fig. 19,** the changes of the index with arc voltage are shown for several values of arc current.

The index has the minimum value at a certain arc voltage for each value of arc current. In the studies done so far, the groove depth is kept constant at 15 [mm].

The effect of the groove depth on the index is investigated. **Figure 20** shows that the index increases as the groove depth decreases and this tendency becomes more apparent as arc power increases.

The outside of the groove is illuminated owing to

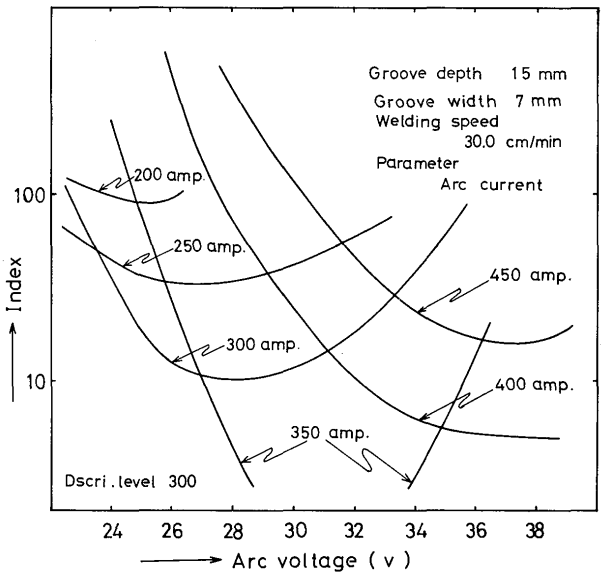

Fig. 19. Dependence of index on arc voltage and arc current.

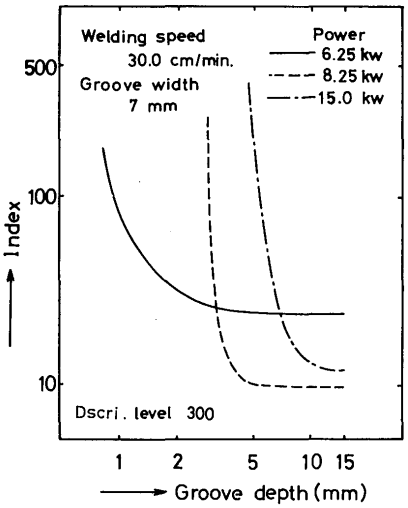

Fig. 20. Dependence of index on groove depth and arc power.

the overflow of the arc flame from the groove zone and to the excess melting if the groove depth is too small for the arc power. The image in this situation is shown in **Photo. 8.**

When the weld line is a curve, its curvature affects the joint configuration sensing. **Figure 21** shows the drawing of an oblique view, where the square groove whose weld line is in a circular arc, and whose radius of curvature is R, groove width is B, groove depth is D, is sighted at an aiming angle in a vertical plane φ, and where φ=50 [°], R=50 [mm], B=7 [mm] and D =28 [mm] in (a), φ=25 [°], R=100 [mm]. B=7 [mm] and D=28 [mm] in (b). The shadowed portion in this figure is the projection of the groove configuration to the plane perpendicular to the line of sight. This portion is thrown on the focusing screen of the pattern

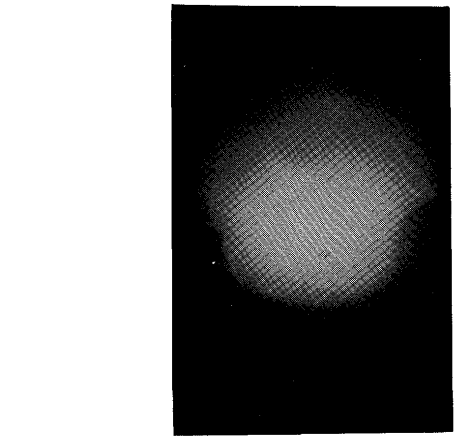

Photo. 8. Image for too small groove depth.

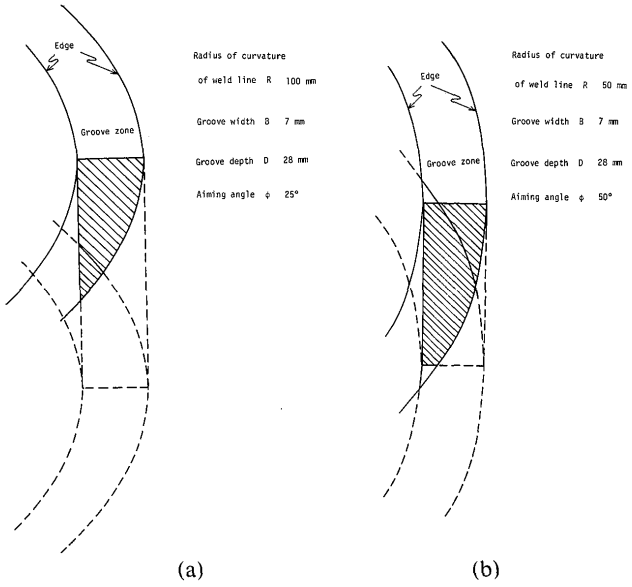

Fig. 21. Illustratings for groove configuration when weld line is curved.

receiver by the light emitted from the welding arc which is generated at the bottom of the groove so that image expresses the more correct groove configuration, if a larger part of the bottom image is included in this shadowed portion. This is investigated quantitatively to some degree. In **Fig. 22,** the curves 1 and 2 are one fourth of ellipses and correspond to the projected images of the outer and inner edges of the

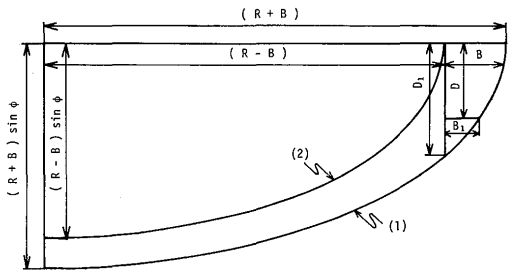

Fig. 22. Drawing to explain joint sensibility when weld line is curved.

groove, width B; in the center the weld line is in a circular arc, its radius of curvature is R, respectively.

If the length D_1 in **Fig. 22** is much larger than the length $D \cdot \cos \varphi$, the projected groove depth, a larger portion of the groove bottom B_b is visible. The image is nearing the correct groove configuration and the reverse case is also true.

Therefore, the ratio $D \cdot \cos \varphi / D_1$ is the sensibility index for the curved weld line. D_1 can be calculated as a function of R, B and φ from eq. 2 which is derived from the primary arithmetic operation.

$$D_1 = \sqrt{2 \cdot B \cdot R} \cdot \sin \varphi \quad \text{---------- (2)}$$

D_2 is defined as follows,

$$D_2 = D_1 / \cos \varphi = \sqrt{2 \cdot B \cdot R} \cdot \tan \varphi \quad \text{---------- (3)}$$

By comparing the given groove depth D with D_2, the sensibility index can be estimated.

Figure 23 shows the relation between $B \cdot R$ and D_2 at constant φ for several values of φ.

Some examples of the groove image are shown in **Photo. 9,** to which the value D/D_2 is written in also.

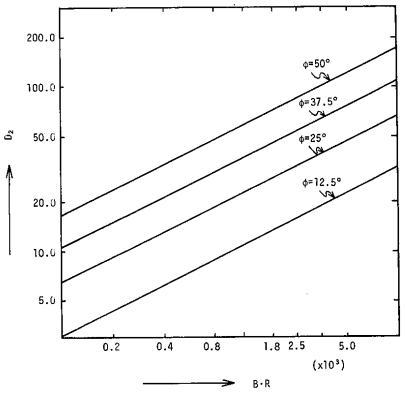

Fig. 23. Relationship between $B \cdot R$ and D_2.

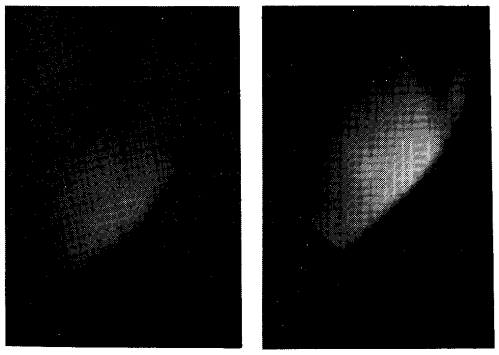

(a) (b)

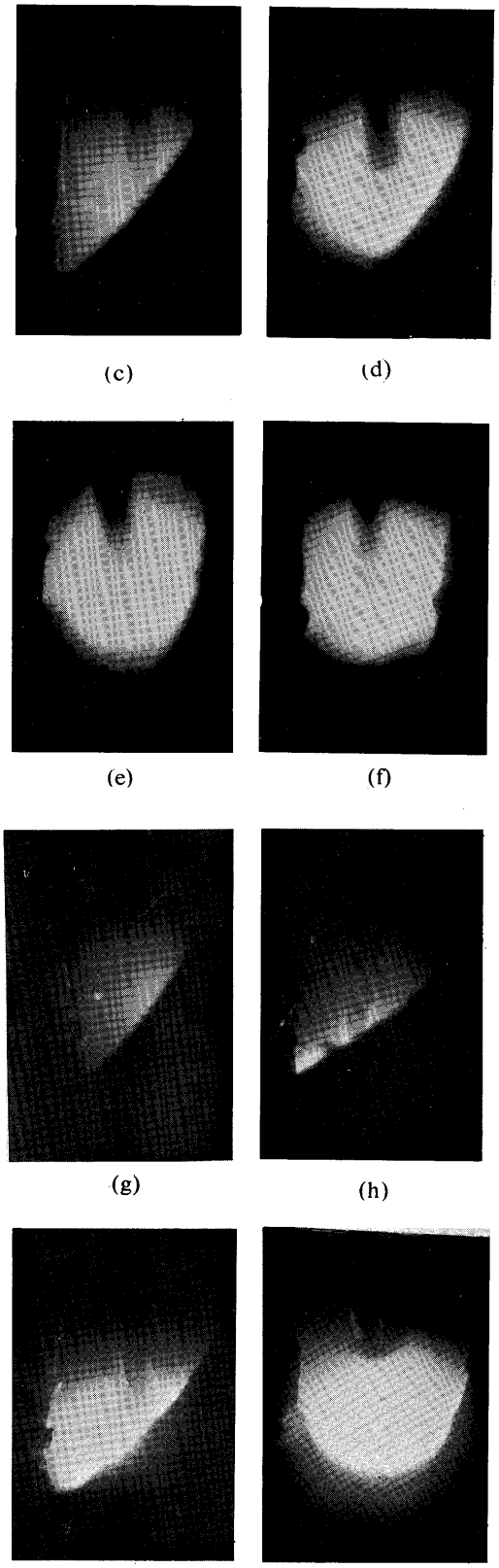

(c) (d)

(e) (f)

(g) (h)

(i) (j)

Photo. 9. Images for curved weld line - Effect of D/D_2
(a) D/D_2=0.44 (b) D/D_2=0.54 (c) D/D_2=0.62
(d) D/D_2=1.13 (e) D/D_2=1.38 (f) D/D_2=1.59
(g) D/D_2=0.49 (h) D/D_2=0.59 (i) D/D_2=1.05
(j) D/D_2=1.42

It is seen from these photographs that the above mentioned fact as to D/D_2 is held for almost all cases.

4. The Structure of the Sensing System and Its Characteristics

The image to be sensed has the characteristics mentioned in the preceding chapter so that the photoelectric elements should be arranged two dimensionally on the focusing screen of the pattern receiver to obtain the information from the portion of the image which has the highest sensitivity.

Figure 24 shows such an arrangement. Each photoelectric element is 7[mm]×2.2[mm] in dimension. As the image on the screen has a magnifications of 4.5, the spatial resolution of these sensitive elements is less than 0.5 [mm].

All the photoelectric elements have serial numbers for convenience and are connected to the voltage comparators which then constitute the light comparators.

Figure 25 shows the connection diagram of the light comparator. The discriminating level of the light comparator is set up arbitrarily with the variable resistance described in **Fig. 25.** Appropriate level setting is indispensable for the proper sensing, as is known from characteristics of the groove image.

Figure 26 show an example of the output signals of the light comparators No. 1～No. 20, when the image is thrown on the screen by stationary TIG arc

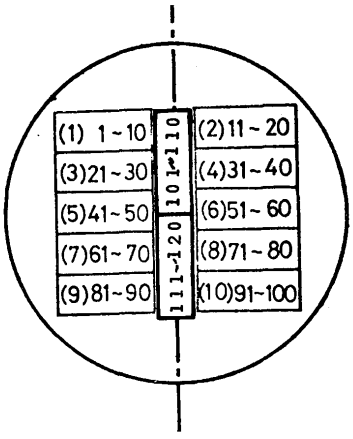

Fig. 24. Arrangement of photoelectric elements on focusing screen.

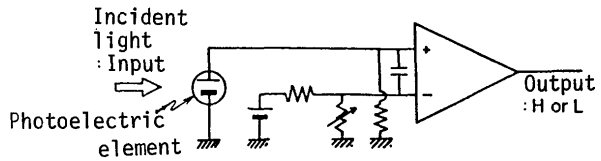

Fig. 25. Connection diagram of light comparator.

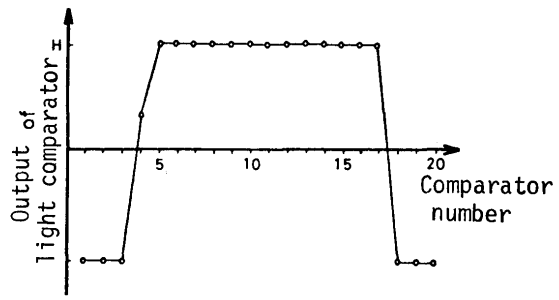

Fig. 26. Example of output signals of light comparatos.

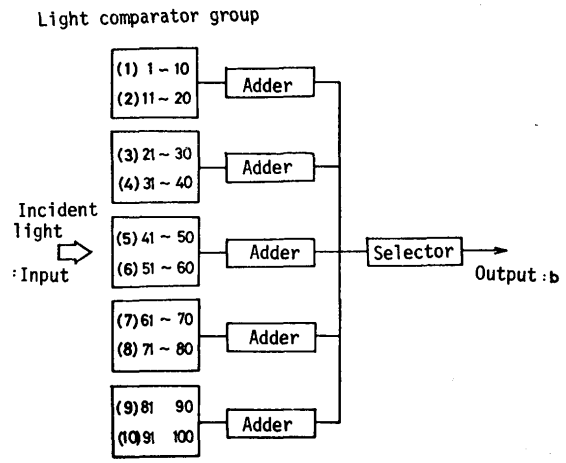

Fig. 27. Block diagram of "b sensor".

on the sequare grooved copper work piece model. The output signals corresponding to the bright and dark part indicate H and L level respectively. The summation of the number of the light comparator which is in H level is equivalent to the groove width. The circuit for indicating the maximum bright part width of the image should be composed as a "b sensor". **Figure 27** shows the block diagram of the "b sensor". The signals from the sensitive elements entor the adders through light comparators. Each output signal of the five adders indicates the total number of the comparators which are in H level on that row and is equivalent to the groove width at that place. The selector can present the maximum voltage among the outputs of the five adders, therefore, its output signal indicates the "b value".

The "b sensing" in this method may cause an error if the groove depth is too small for arc power, or if arc voltage is too low for arc current so that the welding condition must be set appropriately for the sake of accurate sensing. In the "e sensing", horizontal shift of the image on the screen should be detected. **Figure 28** shows the block diagram of the "e sensor". The added output signal of the light comparator groups which exist on the same side in regard to the center line of the screen enters

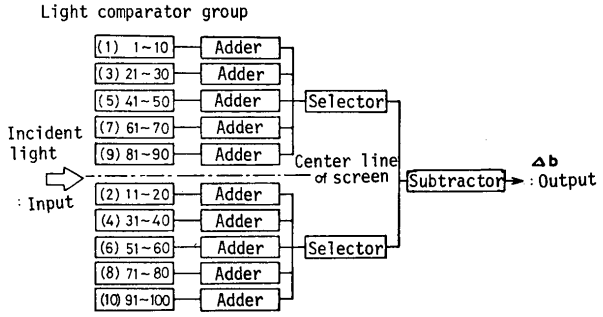

Fig. 28. Block diagram of "e sensor"

each selector. The function of the selector is the same as shown in **Fig. 27.** The output signal of each selector indicates the most external position of the bright image on each side respectively, therefore, the output difference between both selectors indicates the "b value".

When the orthographic projection of the optical axis of the pattern receiver and the welding direction are at an angle of θ_1 as shown in **Fig. 29 (a),** the image on the screen appears as shown in **(b)** of this figure. Two practical examples are shown in **Photo. 10 (a)** and **(b),** the former is the image by TIG arc and the latter is by CO_2 arc.

If θ_1 is not equal to zero, "B value" and "E value" can not be sensed accurately. Then, θ must be always kept at zero. For this purpose, the "θ sensing" is needed. The "θ sensing" can be made by groove tracking of the "θ sensor" which is

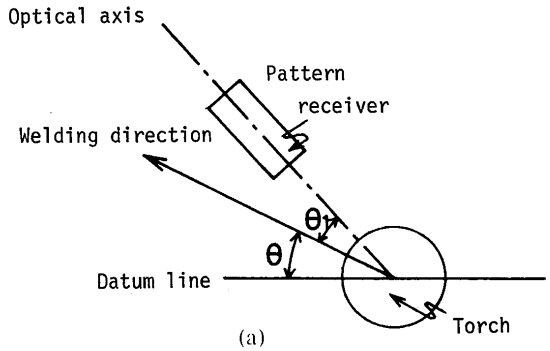

(a)

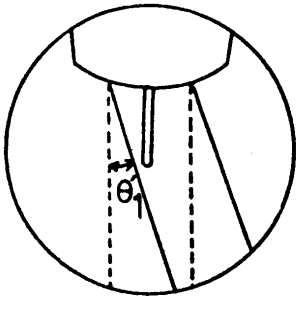

(b)

Fig. 29 (a) Definition for θ and θ_1.
(b) Typical pattern when θ_1 is not equal to zero.

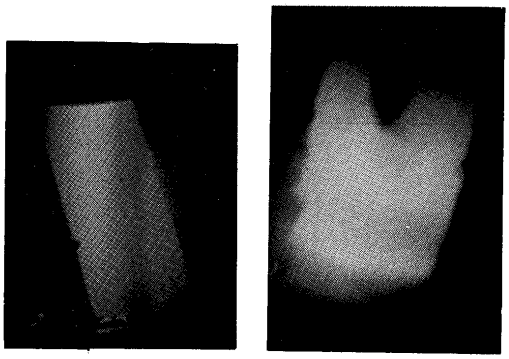

(a) (b)

Photo. 10. Image when θ_1 is not equal to zero.
(a) Image by TIG arc (b) Image by CO_2 arc

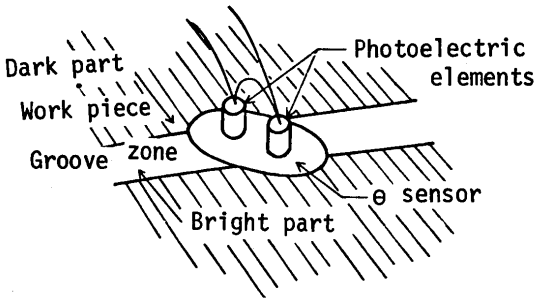

(a)

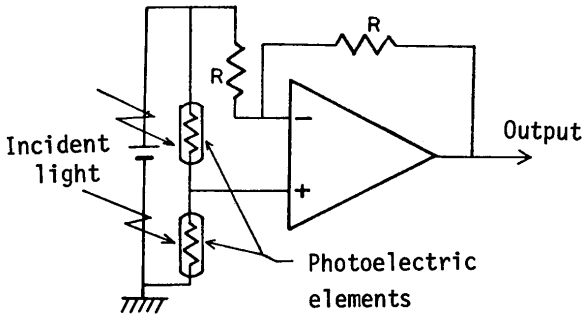

(b)

Fig. 30 (a) Principle of "θ sensor".
(b) Connection diagram of "θ sensor".

attached to the pattern receiver. **Figure 30 (a)** illustrates the principle of the "θ sensor". **Figure 30 (b)** is the diagram of its connection.

The "θ sensor" is located about 80 [mm] in front of the welding head, where the groove zone is illuminated by the random reflection of the light by the fume as shown in **Photo. 11.**

A pair of the photoelectric elements in the "θ sensor" catch the light from the groove zone.

If θ_1 becomes different from zero, the center of the "θ sensor" is apart from the center of the groove zone and the incident light to the pair of photoelectric elements is off balance. The servo-motor is driven by

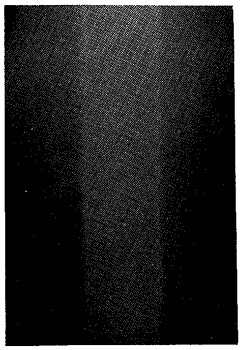

Photo. 11. Image of illuminated groove zone at the front of arc.

the output signal of the "θ sensor" and regulates the plane angle of the pattern receiver so that θ_1 is always kept nearly equal to zero and the orthographic projection of the optical axis coincides with the welding direction; as a result, it is at an angle θ to the datum line. At the same time, a resolver is rotated by the servo-motor to the angle θ. The output voltage of the resolver is proportional to cos θ. The datum line direction component of the welding speed is controlled by this output voltage.

The "Z_1 sensing" is made in the similar method, by which the molten pool was monitored, as described in the previous report in detail.[4] The difference between the molten pool monitoring and the "z_1 sensing" is that the former is made from the back of the arc, while, the latter is made from the front. The photoelectric elements of there serial numbers No. 101~No. 120 (see **Fig. 24**) are used as the sensitive element for the "z_1 sensing".

Sensitivity was calibrated, and reproducibility was checked about these sensors. The sensitive elements being installed at the pattern receiver, output signals from the sensors were recorded in oscillographs when welds were made on the work piece. The results obtained from these oscillograph recordings are plotted on the graphs as shown in **Fig. 31 (a), (b)** and **(c)** which are the calibration of "e sensor", "b sensor" and "θ_1 sensor" respectively. The z_1 sensor has the same sensibility as was shown in **Fig. 10** of the previous report. Their accuracy is satisfactory in practical application.

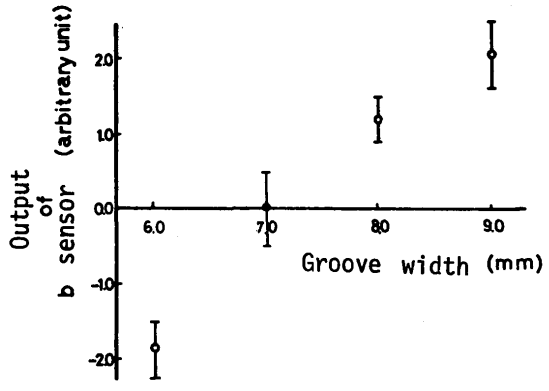

(a)

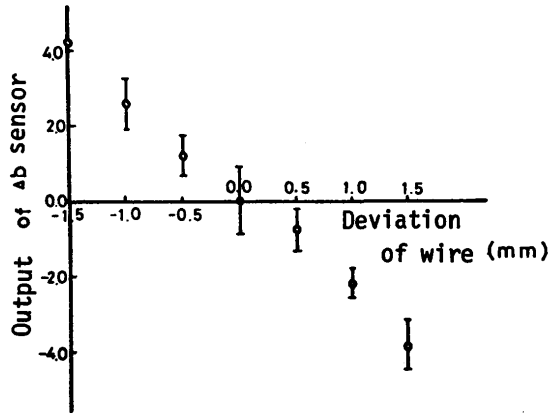

(b)

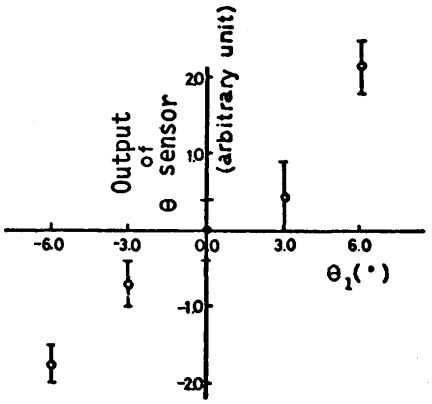

(c)

Fig. 31 (a) Calibration for "b sensor".
(b) Calibration for "e sensor".
(c) Calibration for "θ sensor".

5. Conclusion

1. The joint configuration can be sensed by a new optical method in which the simple optical instrument and the photoelectric elements are used.
2. The principle of this sensing method can be illustrated by the simple drawing, and is most suitable for the square groove.
3. Sensing ability of this method depends upon the various factors of welding parameters. The sensing ability is estimated on these factors by the index calculated from the particularly defined formula.
4. The effect of the curvature of the weld line on the joint (groove) configuration is investigated and the simple relation among the parameters is clarified.
5. The groove width sensor ("b sensor"), the wire deviation sensor ("e sensor"), the weld line deflection sensor ("θ_1 sensor") and the nozzle clearance sensor ("z_1 sensor") are structured based on the

investigated results. The results of calibration on these sensors are satisfactory.

6. The next step is to create an automatic control system utilizing these sensors, and to make joint tracking and weld adapting experiments in order to improve this method for practical application.

Acknowledgment

Thanks are due to Komatsu Co., Ltd. for supplying the instruments and material and also due to Mr. M. Morita for help with experiments.

References

1) M. S. L'vov, A. P. Igoshin and V. B. Surkov: "Method of Compensation for an Error in Height at the Edge of a Joint in Tracking System for Arc Welding", Svov. Pros., (1969), No. 9, 42s～43s.
2) W. A. Wall and D. L. Stephens: "Automatic Closed Circuit Television Electrode Guidance for Welding", W. J., (1969), No. 9, 713s～720s.
3) S. A. Kolynbakin, Yu. A. Pachentsev and B. A. Steblovkin: "An Automatic System for Guiding the Electrode along Butt Joints during Argon Tungsten Arc Welding", Avt. Svarka, (1969), No. 10, 52s～55s.
4) Y. Arata and K. Inoue: "Automatic Control of Arc Welding by Monitoring Molten Pool", Transaction of JWRI, (1972), No. 1, 99s～113s.